Eur. Phys. J. B (2024) 97:35
https://doi.org/10.1140/epjb/s10051-024-00670-y

THE EUROPEAN PHYSICAL JOURNAL B

Regular Article - Solid State and Materials

In-depth study of dielectric properties of iron chloride embedded polyaniline nanocomposites

Geeta Gulati[1], Meenakshi[1], Asha[2,a], Rachna Dhankhar[3], Sonia[1], Rishi Pal[4], and Supreet[5]

[1] Department of Physics, Baba Mastnath University, Asthal Bohar, Rohtak, Haryana 124021, India
[2] Department of Basic and Applied Sciences, Bhagat Phool Singh Mahila Vishwavidyalaya, Khanpur Kalan, Sonipat, Haryana 131305, India
[3] Department of Chemistry, Maharshi Dayanand University, Rohtak, Haryana 124001, India
[4] Department of Applied Science, Kalpana Chawla Government Polytechnic for Women, Ambala, Haryana 134003, India
[5] Department of Physics, Amity School of Applied Sciences, Amity University, Gurugram, Haryana 122413, India

Received 27 December 2023 / Accepted 11 March 2024 / Published online 30 March 2024

Abstract. In the present research work, the pristine polyaniline and iron chloride-embedded polyaniline nanocomposites were synthesized by adopting the chemical oxidative polymerization route. The AC conductivity and dielectric properties of the titled samples were measured in temperature and frequency range of 173–373 K and 100 mHz to 1 MHz, respectively. The result reveals that the dielectric constant of synthesized samples increases as temperature increases whereas it decreases with an increase in applied frequency. The dielectric constant of pristine polyaniline found to be ∼ 497 which attains value ∼ 875 on the addition of 25 wt% iron chloride, which indicates that dielectric properties are strongly affected by the doping of iron chloride. In addition to that various theoretical models such as Arrhenius model, Jonscher power law, etc. were employed to analyze the charge transport mechanism. The low value of AC conductivity signifies its strong dependency on both frequency and temperature. AC conductivity increases with the increase in operating temperature as well as applied frequency, which may be attributed to the increase in the concentration of iron chloride trapped charge carriers.

1 Introduction

Polyaniline (PANI) has fascinated researchers worldwide over the last few decades due to its remarkable physical and chemical properties, including low cost, ease of fabrication, outstanding environmental durability, adjustable electrical conductivity, good redox activity, high yield, and many more [1–3]. It comes under the category of polymers, which were considered insulators due to the non-availability of free electrons before 1974. But later on, in 2000, Shirakawa was awarded the Nobel Prize for investing the semiconductor properties of polymers for the first time [4–9] and named them conducting polymers. Therefore, physicists, chemists, and material scientists are now very interested in PANI, one of the many conducting polymers, due to its diverse applications in industries such as electrodes for sensors, conductive films for LEDs, etc. [10–12]. The chemical structure of polyaniline consists of a flexible NH group on either side of a phenylene ring that is connected to a polymer chain. And the presence of this adaptable NH group affects the physical, electrical, and chemical properties of polyaniline. Moreover, PANI can be synthesized by chemical oxidative polymerization. It is easily obtained in its various forms, such as emeraldine salt and base form, with good environmental stability and conductivity. The range of conductivity of these polymers depends on the type and concentration of doping used in the pure material and can change from semiconductor to conductor. Therefore, the incorporation of nanoparticles in polymer matrices led to the production of nanocomposites with enhanced conductive properties. Due to the addition of a modest fraction of nanoscale fillers, transition metal oxides, halides, and nitrates, PANI nanocomposites exhibit a significant improvement in their thermal, mechanical, optical, and electrical properties. Based on impedance measurements, Kulkarni et al. [13] examined the NH_3 sensing behaviour of a flexible PANI-WO_3 sensor. A greater understanding of the interpolymerization process used to create regular nanoparticles for PANI was provided by Mezan et al. [14]. These days, there is a growing interest in the dielectric and charge transport studies of conjugated polymers due to their implementation in electronic gadgets. In the dielectric measurements, the short-range AC conductivity of the conjugated polymers is controlled by the relaxation of the applied electric field. Dielectric relaxation spectroscopy

[a] e-mail: arana5752@gmail.com (corresponding author)

is used to study the relaxation phenomenon and electrical properties of conjugated polymers. The dielectric properties and charge transport process of conducting polymers are impacted by this relaxation. A thorough understanding of the DC/AC conduction mechanism is essential due to the wide range of applications for these devices. Earlier, various researchers have worked on the dielectric properties of various conducting polymers [15–18]. Pal et al. [15] investigated the dielectric properties of reduced MWCNTs embedded PANI composite sample. This sample exhibits the high value of dielectric constant i.e. ~ 1170. PANI/TiO_2 contains the lower values of the dielectric constant prepared by Mo et al. [16]. However, Das et al. [17] reveals that the synthesized PANI/Sulfonic Acid nanocomposites exhibit higher values of dielectric constant i.e., 5×10^3. However, the long-range temperature based dielectric properties of chloride-based dopants embedded polyaniline composite samples have not been reported. Therefore, in the present paper we aimed to comprehend how an iron chloride ($FeCl_3$) particle in the polyaniline geometry affects the dielectric and charge transport characteristics.

2 Experimental details

2.1 Synthesis of pristine and $FeCl_3$-embedded PANI nanocomposite samples

Initially, the chemicals were purchased from Sigma Aldrich for the preparation of pure and nanocomposites samples. After that, two aqueous solutions of oxidant (ammonium persulphate: APS) and monomer (aniline hydrochloride) were prepared identically with 25 and 20 mM concentrations, respectively. Further both the solutions were kept in the ice bath for one hour and the temperature was maintained below 4 °C. Then the oxidant solution was kept on an ice bath to maintain the lower temperature, then pre-cooled monomer solution was added in it dropwise along with the 1 M HCl and allowed to complete polymerization reaction for overnight. Next day, the obtained solution was filtered using the Whatman filter paper. The obtained yield was firstly dried in air and after that kept in oven at temperature ~ 50 °C to remove the moisture inside it. After getting the dried salt, it crushed into a fine powder using Agate mortar and named it as N0. Moreover, for the preparation of $FeCl_3$-embedded PANI nanocomposite samples, the above-mentioned process was followed with doping concentration 10, 15, 20 and 25 wt% of $FeCl_3$ and named as N1, N2, N3 and N4, respectively.

2.2 Analytical techniques

AC conductivity and dielectric measurements of the synthesized samples were carried out in the frequency and temperature range of 0.1–1 MHz and 173–373 K. To carry out the measurements, the powder samples were converted in 10 mm diameter and 1 mm thickness pellets using hydraulic press. After that to make electrodes, silver paste was applied on both sides of the pallet which behaves like a parallel plate capacitor. The measurements were carried out using Novocontrol technologies Broadband Dielectric/Impedance Spectrometer (ALPHA-Active Cell V6.57ATB IEC = 10).

3 Results and discussion

3.1 AC conductivity and dielectric measurements

Dielectric study, an electrical property provides detailed information regarding the distribution of electric field within the sample and it is related to the electro-optic property also. Figure 1a–e illustrates the variation in the real part (ε') of permittivity as a function of operating temperature at different frequencies. From the figure it is observed that the dielectric constant decreases with an increase in frequency i.e. at low frequencies, a higher value of the dielectric constant is found which is due to the contribution of all these polarizations. On the other hand, at higher frequencies the low value of the dielectric constant is observed due to the gradual loss of these polarizations. Moreover, there is a deviation in the values of the dielectric constant along with the increase in temperature indicating the strong interaction between Debye-type properties [19–21]. In addition, the values of complex dielectric function change with the frequency as the expression given below:

$$\varepsilon^*(\omega) = \varepsilon'(\omega) - i\varepsilon''(\omega) \quad (1)$$

The complex dielectric function contains different polarizations such as (a) electronic polarization which is associated with the distribution of charge carriers, (b) lattice polarization, which is associated with the mobility of charge carriers, and (c) dipolar polarization which indicates the presence of permanent dipoles and dipole movements due to different types of impurities [22]. At low frequencies, a higher value of the dielectric constant is found which is due to the contribution of all these polarizations. On the other hand, at higher frequencies the low value of the dielectric constant is observed due to the gradual loss of these polarizations. From Fig. 1, it has been observed that the dielectric constant increases gradually at low temperature whereas abruptly at high temperature. This rise in dielectric constant with increased temperature indicates that the polarization ratio and dielectric dispersion both are temperature dependent [23]. Moreover, there is a decrease in the dielectric constant in some cases at higher temperature. This may be due to the presence of impurities or lattice defects. Figure also shows that for lower temperatures and lower frequency values, the values of static dielectric constant (ε_o) is

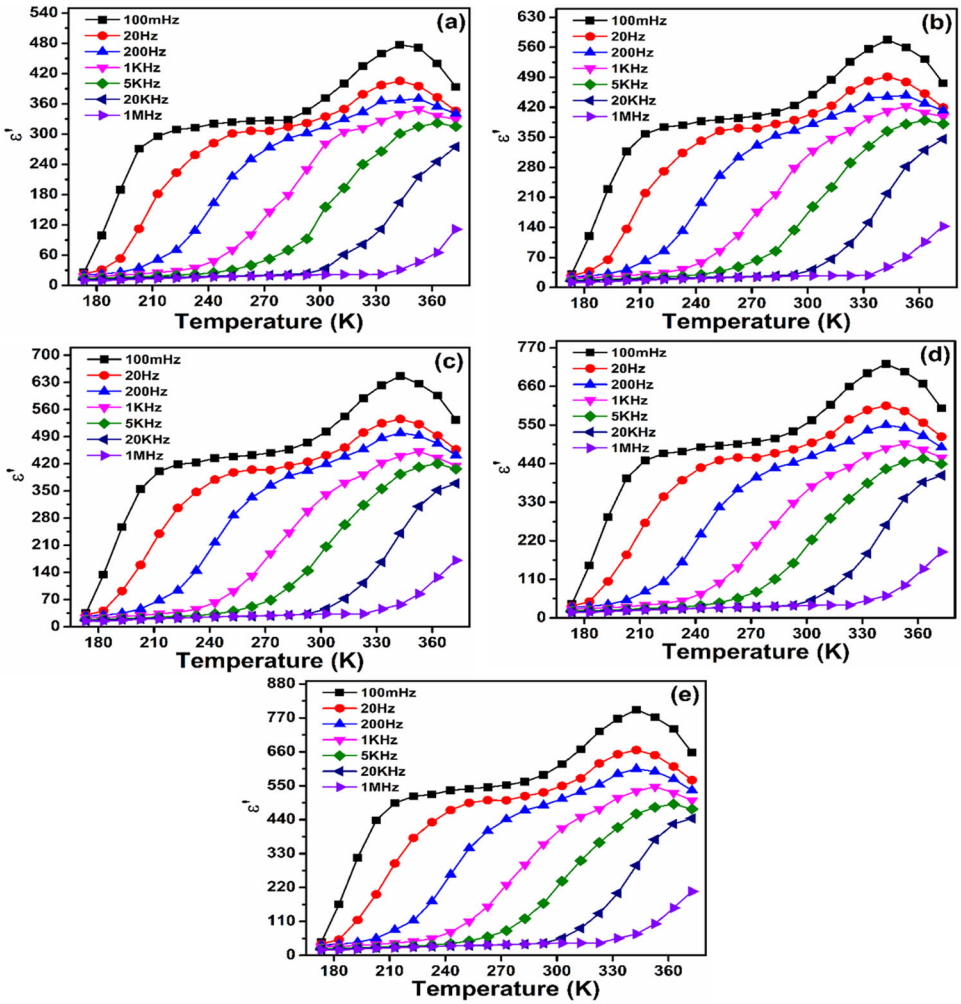

Fig. 1 Dielectric constant versus temperature for **a** pristine PANI, **b** 10 wt%, **c** 15 wt%, **d** 20 wt% and **e** 25 wt% $FeCl_3$ doped PANI samples at different values of frequency

low. The Debye-type relaxation can be given by [23, 24].

The Debye-type relaxation can be given by [23, 24]

$$\varepsilon'(\omega) - \varepsilon_\infty = \frac{\varepsilon_o - \varepsilon_\infty}{\left\{1 + \left(\frac{f}{f_o}\right)^2\right\}} \tag{2}$$

where, f_o, ε_∞ and ε_o are relaxation frequency, high frequency and static dielectric constant, respectively.

Moreover, the graph between the real part of permittivity and frequencies has been also plotted at different temperature as shown in Fig. 2a–e. From the Figs. 1 and 2, it is clear that the values of dielectric constant rise with a rise in temperature whereas reduce with the reduction in applied frequency. The values of the dielectric constant are high at lower values of frequency this may be because of the accumulation of charge carriers at the interfacial region between insulating grain boundary and semiconducting grains and which further leads to Maxwell–Wagner interfacial polarization. This kind of characteristics may lead to a plateau or also this plateau may be due to the presence of iron chloride in the polyaniline matrix. The plateau in the intermediate frequency range shifted towards high-frequency range along with the increase in temperature. However, with the increase in frequency, the dipoles are unable to synchronize along the applied frequency, therefore, polarization will be reduced and hence dielectric constant decrease [25, 26]. The estimated values of dielectric constant at various values of frequencies and temperatures are tabulated in Table 1 for the pristine and $FeCl_3$ doped PANI samples. The observed data resembles already reported work [24, 27–29].

The collected data for conductance (G) at different frequencies and temperature were used to estimate the values of AC conductivity for prepared samples using the following expression [27].

$$\sigma'(\omega) = G(\omega) \times \frac{d}{A} \tag{3}$$

Here, A and d is the cross-sectional area and thickness, respectively. Figure 3a–e depicts the trend of AC conductivity as a function of $1000/T$ at different frequencies. The measured AC conductivity increases

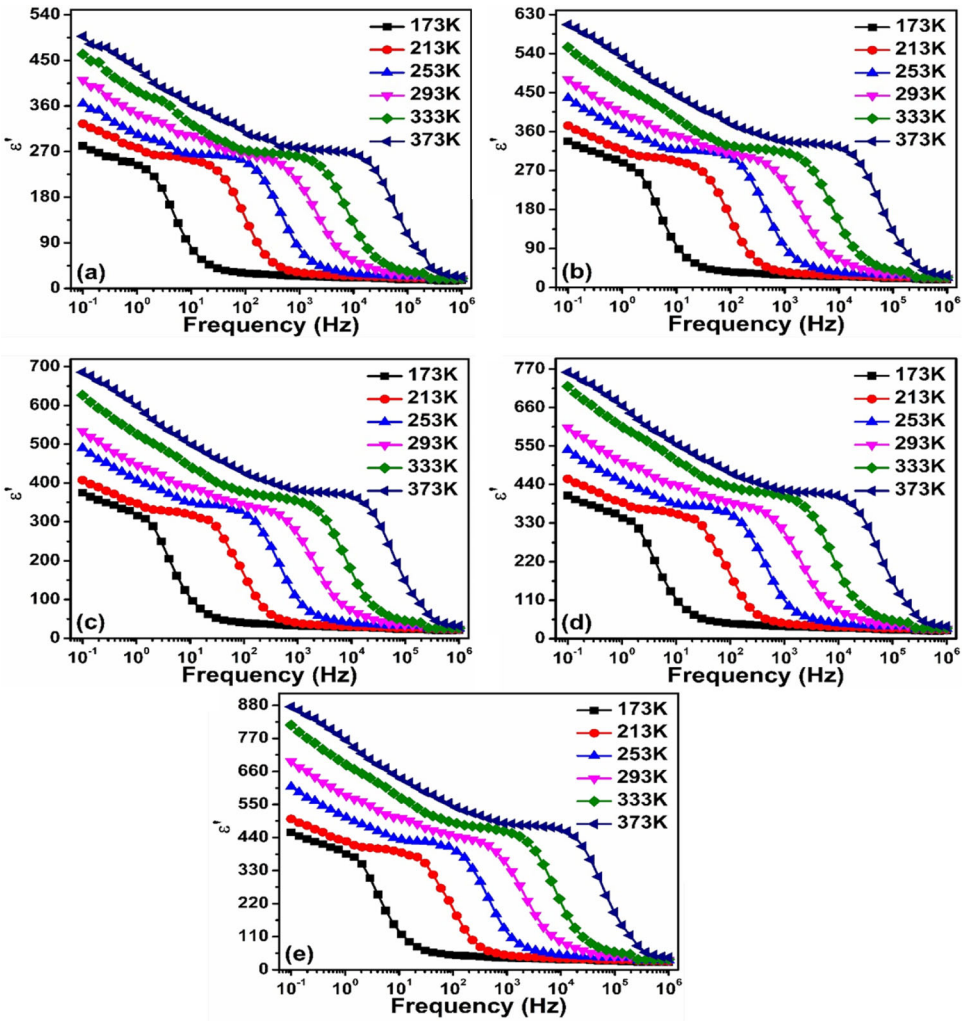

Fig. 2 Dielectric constant versus frequency for **a** pristine PANI, **b** 10 wt%, **c** 15 wt, **d** 20 wt% and **e** 25 wt% $FeCl_3$ doped PANI samples at different values of temperature

as frequency increases while decreasing as $1000/T$ increases. The AC conductivity is strongly influenced by the presence of bound charge carriers and their concentration is found to be high as compared to free charge carriers. It has been observed that free charge carriers help to boost DC conductivity. Thus, the combined electrical conductivity that has been measured or estimated is made up of both AC and DC conductivities [28, 29] as shown by the expression given below.

$$\sigma'(\omega) = \sigma_{\mathrm{dc}} + \sigma(\omega) \tag{4}$$

Here σ_{dc} and $\sigma(\omega)$are DC and AC conductivity, respectively. The values of AC conductivity found to increase with an increase in the frequency and temperature attributed to the increase in bound charge carrier concentration. The variation in AC conductivity w.r.t frequency for the prepared samples at different temperatures has also been examined (Fig. 4a–e). The observed values show a resemblance with already reported work [30–33].

According to Jonscher's universal power law [34, 35], AC conductivity can be calculated by using the equation given below:

$$\sigma'(\omega) = \sigma_{dc}\left[1 + \left(\frac{\omega}{\omega_{\mathrm{H}}}\right)^{s}\right] \tag{5}$$

where ω_{H} is the charge carrier hopping or crossover frequency, and s is the frequency exponent. The interaction between charge carriers is referred to as frequency exponent, and its values should lie between 0 and 1. Equation (5) has been used to theoretically fit the frequency-based conductivity ($\sigma'(\omega)$) at different temperature to determine the values of ω_{H}, σ_{dc} and s. The calculated values of frequency exponent (s) are presented in Table 1. The data that were experimentally fitted provide a good fit with the parameter. The applicability of Jonscher's power law in the presently prepared samples has also been examined at several temperatures, and it is discovered that the pristine and nanocomposites follow the power law through the large temperature range.

Table 1 Various observed and fitted parameters for the pristine and PANI nanocomposite samples

Parameters	Measured values				
	N0	N1	N2	N3	N4
ε' ($T = 373$ K, $f = 100$ mHz)	497.41	606.84	675.73	761.16	875.33
ε'' ($T = 373$ K, $f = 100$ mHz)	393.74	476.41	533.58	597.61	657.37
s ($T = 373$ K, $f = 100$ mHz)	0.76	0.74	0.67	0.61	0.58
H_{f} (eV)	1.93	2.03	2.05	2.34	2.51
H_{m} (eV)	1.18	1.37	1.22	1.45	1.01
$H_{\mathrm{m}} + H_{\mathrm{f}}$ (eV)	3.11	3.40	3.27	3.79	3.52
E_{dc} (eV)	1.27	3.28	3.44	3.33	3.29
W_{m} (eV)	0.80	0.74	0.58	0.49	0.46

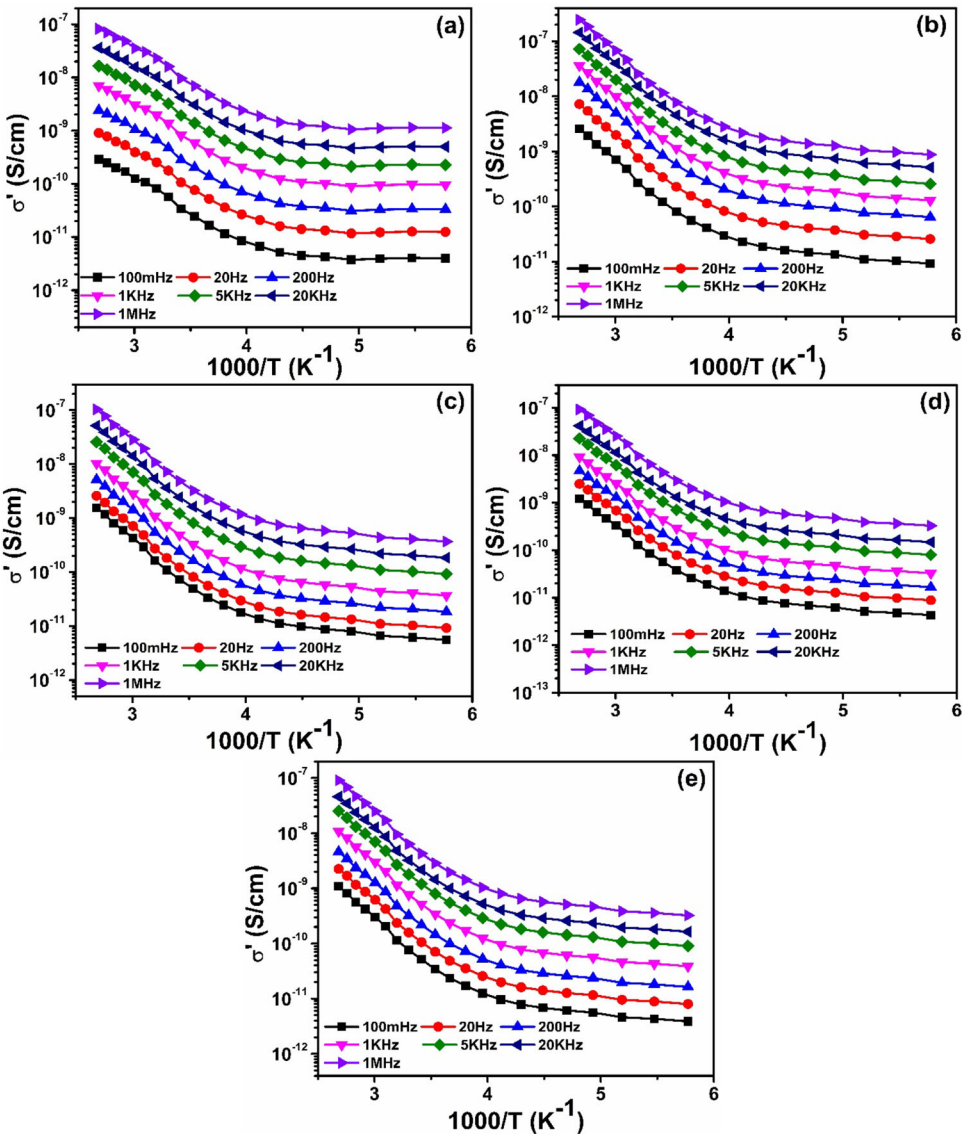

Fig. 3 Variation in measured AC conductivity as function of $1000/T$ for **a** pristine and **b** 10 wt%, **c** 15 wt%, **d** 20 wt% and **e** 25 wt% $FeCl_3$ doped PANI samples at different values of frequency

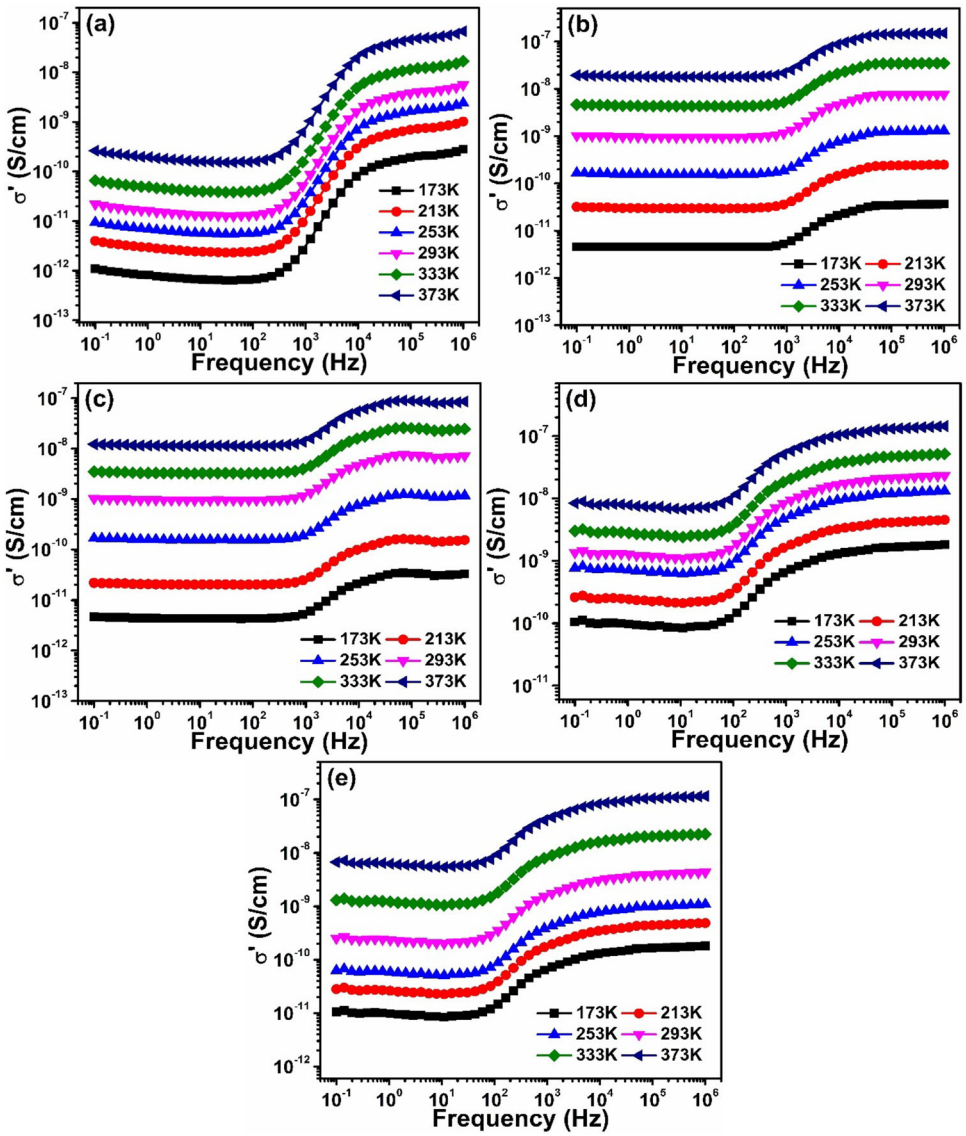

Fig. 4 Variation in logarithmic measured ac conductivity as a function of logarithmic frequency for **a** pristine and **b** 10 wt%, **c** 15 wt%, **d** 20 wt% and **e** 25 wt% $FeCl_3$ doped PANI samples at different values of temperature

The propagated charge carriers (n) from whole charge carriers (N) are determined by using relation:

$$n = N\exp\left(-\frac{G_f}{kT}\right) = N\exp\left(\frac{S_f}{k}\right) \times \exp\left(-\frac{H_f}{kT}\right) \tag{6}$$

where H_f, S_f and G_f stands for enthalpy, entropy and free energy, respectively. The crossover frequency and DC conductivity can be expressed as [36]

$$\omega_H = \omega_o\exp\left(\frac{S_m}{k}\right) \times \exp\left(-\frac{H_m}{kT}\right) \tag{7}$$

and

$$\sigma_{dc} = \frac{NZ^2e^2d^2\gamma\omega_o}{kT}\exp\left(\frac{S_f + S_m}{k}\right) \times \exp\left(-\frac{H_f + H_m}{kT}\right) \tag{8}$$

where γ, H_m, S_m, ω_o and d represent a geometric constant, enthalpy of migration, entropy of migration, attempt frequency and jump distance, respectively. Using the Eqs. (7) and (8), the values of H_m and $H_f + H_m$ are calculated (Table 1), respectively (Fig. 5). The enthalpy of migration is a type of heat energy that is partially used in the ejection of electrons; denoted by H_f, whereas heat energy partially used to transport these charge carriers; denoted by H_m. The values of H_f for all the prepared samples are found to be positive which signifies that concentrations of ejected charge carriers are fewer than overall charge carriers' concentration [36].

At low temperatures, the measured AC conductivity ($\sigma'(\omega)$) found to be higher as compared to dc conductivity (σ_{dc}). Various researchers from worldwide also observe such kind of trend [23, 30–33]. The values of the frequency factor calculated using Eq. (5) also show

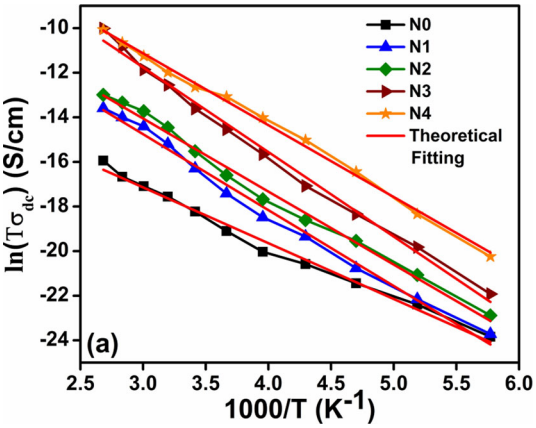

Fig. 5 Linear fitting of **a** $\log(T\sigma_{dc})$ versus $1000/T$ for pristine and $FeCl_3$ doped PANI nanocomposite samples

the reduction in its value at higher values of temperature and lower values of frequency. These results indicate towards the dominant behavior of free charge conductivity [37]. Moreover, the frequency exponent 's' also depends on temperature. The dependency of values of 's' on temperature indicates the applicability of the quantum mechanical tunnelling (QMT) model for charge carrier's propagation across the potential barriers is disregarded. Therefore, the Pike's relation can be used to express the temperature-dependent variation of 's' [38–40].

$$1 - s = \frac{6k_BT}{W_m} \tag{9}$$

If the value of 's' is unity, then the factor $6k_BT/W_m$ should be equal to zero which is not possible practically. However, putting the values of 's' factor, the values of polarons binding energy (W_m) can be calculated using the expression (9), and the calculated values of W_m at room temperature are depicted in Table 1. The sustainability of the classical hopping conduction (CHC) model may be investigated using the density of states across the fermi level. However, the density of states ($N(E_F)$) across the fermi level gives the values of conductivity through the Mott and Austin [41] expression

$$\sigma(\omega) = \left(\frac{\pi}{3}\right)e^2k_BT\{N(E_F)\}^2\left(\frac{\omega}{\alpha^5}\right)\left\{\ln\left(\frac{\nu_{ph}}{\omega}\right)\right\}^4 \tag{10}$$

Here, υ_{ph} and α are phonon frequency and electronic wave function decay constant, respectively. The concentration of density of states for pristine PANI are found to be 3.97×10^{21} and 4.63×10^{20} eV^{-1} cm^{-3} at 100 mHz and 1 MHz frequencies, respectively, at a fixed temperature (173 K). At lower temperatures, these specific $N(E_F)$ numbers indicate that charge carriers are transit hopping [36]. The uncorrelated hopping through the pair of sites follows through the Eq. (10), and are used to calculate values of density of states [24]

$$\alpha^{-1}\left\{\ln\left(\frac{\nu_{ph}}{\omega}\right)\right\} < \left\{\frac{4\pi}{3}N(E_F)k_BT\right\}^{\frac{1}{3}} \tag{11}$$

The large number of density of states corresponds to the rise in delocalization of electronic states through the forbidden gap which indicates the increase in a measured value of AC conductivity. The plotting between $\sigma'(\omega)$ and ω is nearly similar to the theoretical fitting of obtained conductivity data using expression (5). Therefore, the relation between σ_{dc} and ω_H can be obtained by solving expression (7) and (8) [36].

$$\sigma_{dc} = \frac{NZ^2e^2d^2\gamma\omega_H}{kT}\exp\left(\frac{S_f}{k}\right) \times \exp\left(-\frac{H_f}{kT}\right) \tag{12}$$

From the Eq. (12), the σ_{dc} varies linearly with enhancement in ω_H and that follow the Barton–Nakajima–Namikawa (BNN) relation [42, 43]

$$\sigma_{dc} = p\Delta\varepsilon\varepsilon_o\omega_m \tag{13}$$

where, $\Delta\varepsilon = \varepsilon_s - \varepsilon_\infty$, p, ω_m, ε_o, dielectric loss peak frequency, permittivity of free space, dielectric constant at higher values of frequency and static dielectric constant, respectively. Where ε_∞ and ε_s are constant. The factor '$\Delta\varepsilon$' strongly subjected to temperature in the BNN expression. The linear nature of the plot between $\log\sigma_{dc}$ versus $\log\omega_H$ reveals the validation of the BNN model (Fig. 6a). This also indicates that both DC and AC-type charge transport mechanisms are associated with present samples [44].

The activation energy can be calculated using expression through the Arrhenius model [45]

$$\sigma_{dc} = \sigma_o\exp\left(-\frac{E_{dc}}{kT}\right) \tag{14}$$

Here k, σ_o and E_{dc} are Boltzmann constant, pre-exponential factor and activation energy, respectively. A graph between $\ln(\sigma_{dc})$ and $1000/T$ is used to evaluate the values of activation energy and check the applicability of the Arrhenius model, as illustrated in Fig. 7b. It should be linear, But for the present samples this is not linear for all the samples which discarded the validation of Arrhenius model for the dc charge transport mechanism. However, the estimated quantities of activation energy are present in Table 1.

To comprehend the conduction behavior in the synthesized samples, the imaginary part of permittivity has also been explored through the use of the following statement [46].

$$\varepsilon''_{ac} = \frac{\sigma(\omega)}{\omega\varepsilon_o} \tag{15}$$

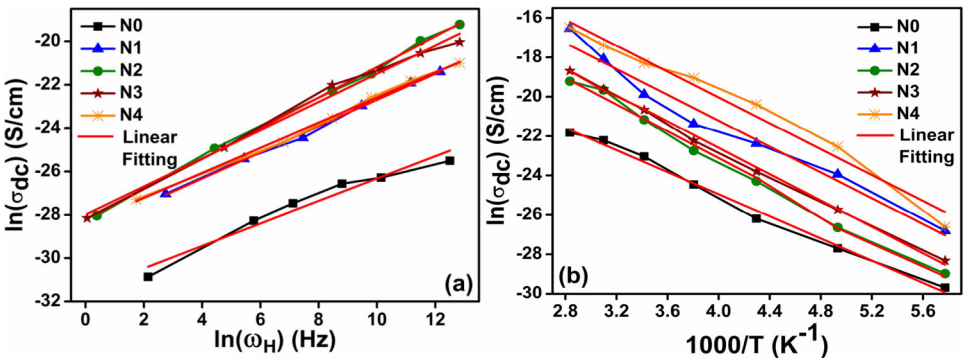

Fig. 6 Variation in $\log\sigma_{dc}$ versus **a** $\log\omega_H$ and **b** $1000/T$ for pristine PANI and $FeCl_3$ doped PANI nanocomposite samples

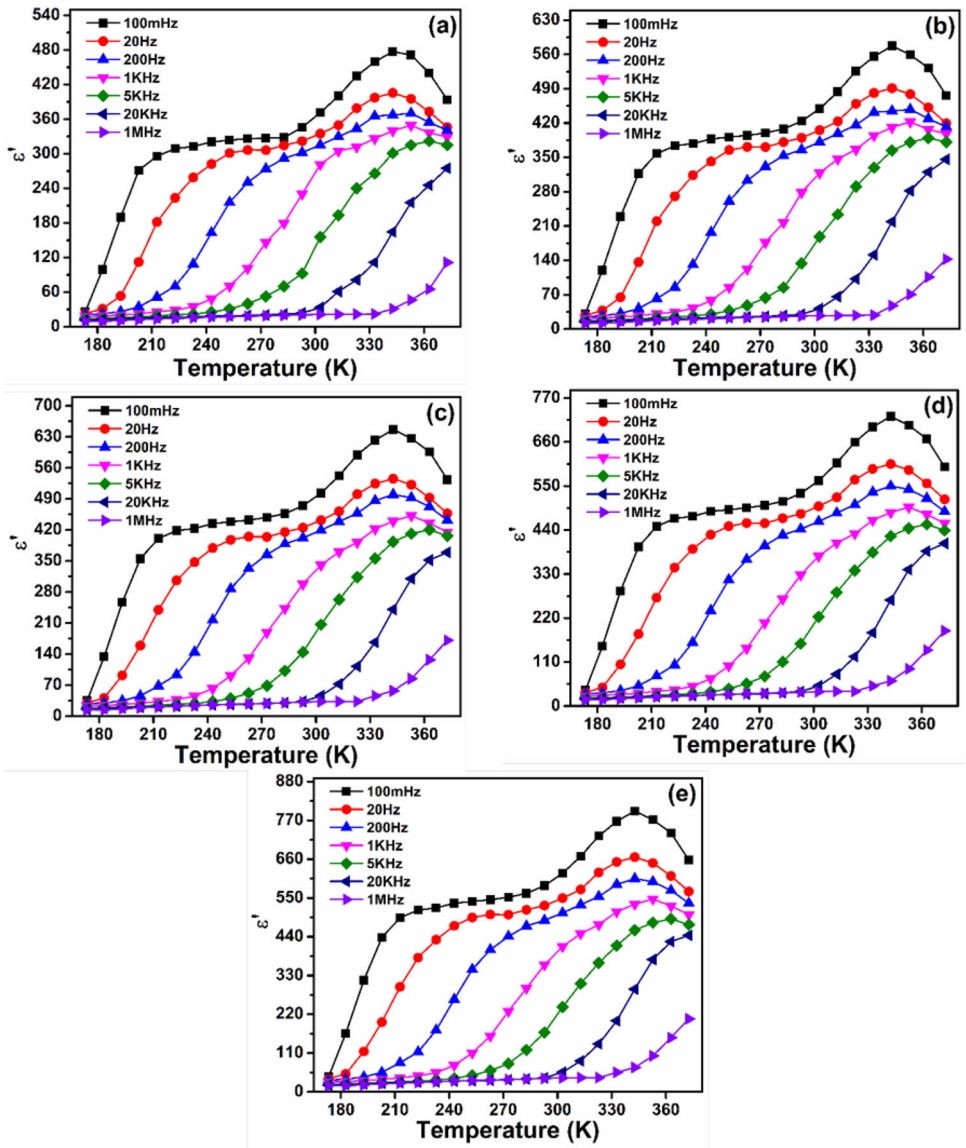

Fig. 7 Dielectric loss versus temperature at various frequencies for **a** pristine PANI, **b** 10 wt%, **c** 15 wt%, **d** 20 wt% and **e** 25 wt% $FeCl_3$ doped PANI

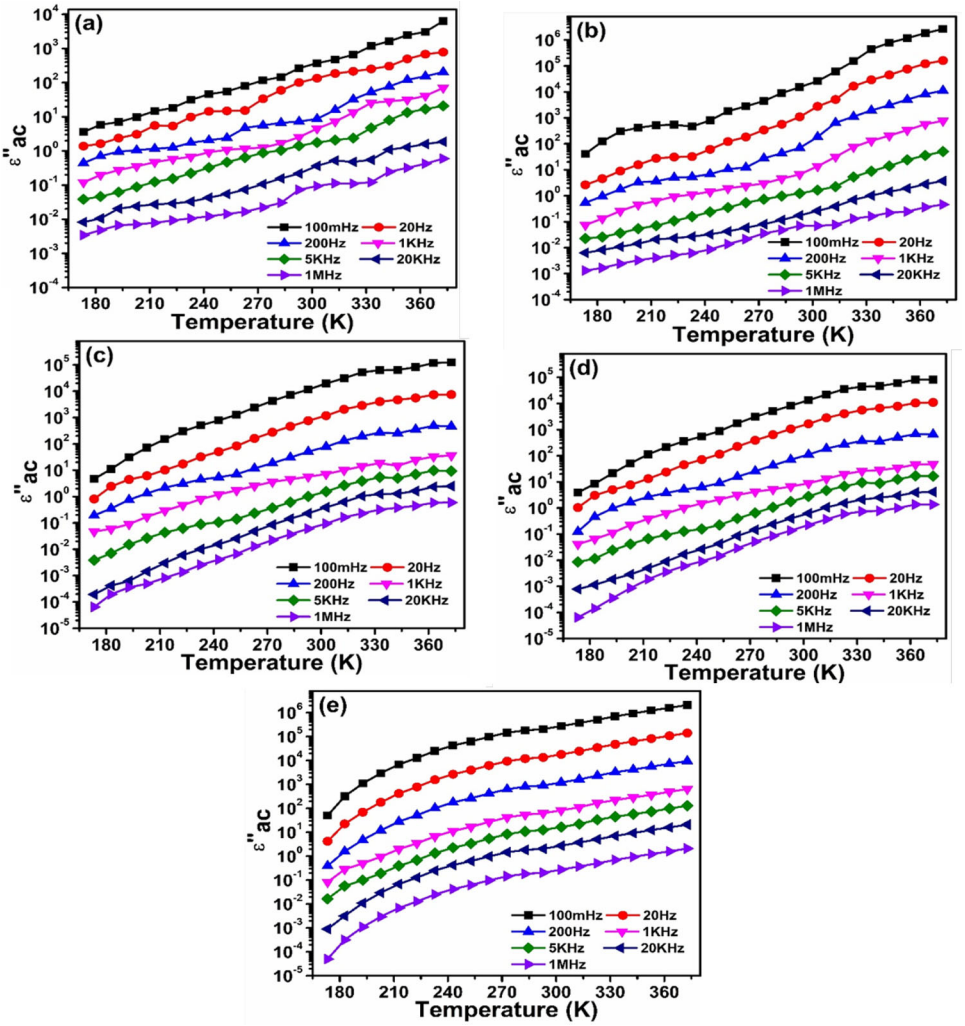

Fig. 8 Dielectric loss versus frequency at various temperatures for **a** pristine PANI, **b** 10 wt%, **c** 15 wt%, **d** 20 wt% and **e** 25 wt% $FeCl_3$ doped PANI

The alteration in behavior of dielectric loss w.r.t. the temperature and frequency are shown in Figs. 7a–e and 8a–e, and observed that the dielectric loss rises with a rise in temperature while decreasing with a rise in frequency. Besides, at the specified temperature and frequency range for prepared nanocomposite, no Debye-type pigmentation peak is detected, unlike in the case of the dielectric constant.

When it becomes challenging to comprehend conduction behavior through complex permittivity, electric modulus formalism is then added to explain the space charge relaxation mechanism. According to this formalization, the complex electric modulus (M*) is known as the reciprocal of complex permittivity using the expression given below [47].

$$M^* = \frac{1}{\varepsilon^*} \tag{16}$$

and

$$M^* = M' + M'' = \frac{\varepsilon'}{(\varepsilon')^2 + (\varepsilon'')^2} + \frac{\varepsilon''}{(\varepsilon')^2 + (\varepsilon'')^2} \tag{17}$$

where M'' and M' are imaginary and real components of electric modulus, respectively. The energy loss and constant caused by the applied electric field are indicated by the imaginary and real parts of the electric modulus. As seen in Fig. 9a–e, the real part of the electric modulus is represented w.r.t. to applied frequency. The M'' may be pronounced as the relaxation functioned $\varphi(t)$ Fourier transport [47]

$$M^* = M_\infty \left[1 - \int_0^\infty \exp(-\omega t)\left(\frac{\mathrm{d}\varphi}{\mathrm{d}t}\right)\mathrm{d}t\right] \tag{18}$$

The time-evaluated electric field for the present samples is denoted by $\varphi(t)$, and also defined as the Kohlrausche–Williamse–Watts (KWW) model [48].

$$\varphi(t) = \exp\left[-\left(\frac{t}{\tau_\mathrm{m}}\right)\right]^\beta \tag{19}$$

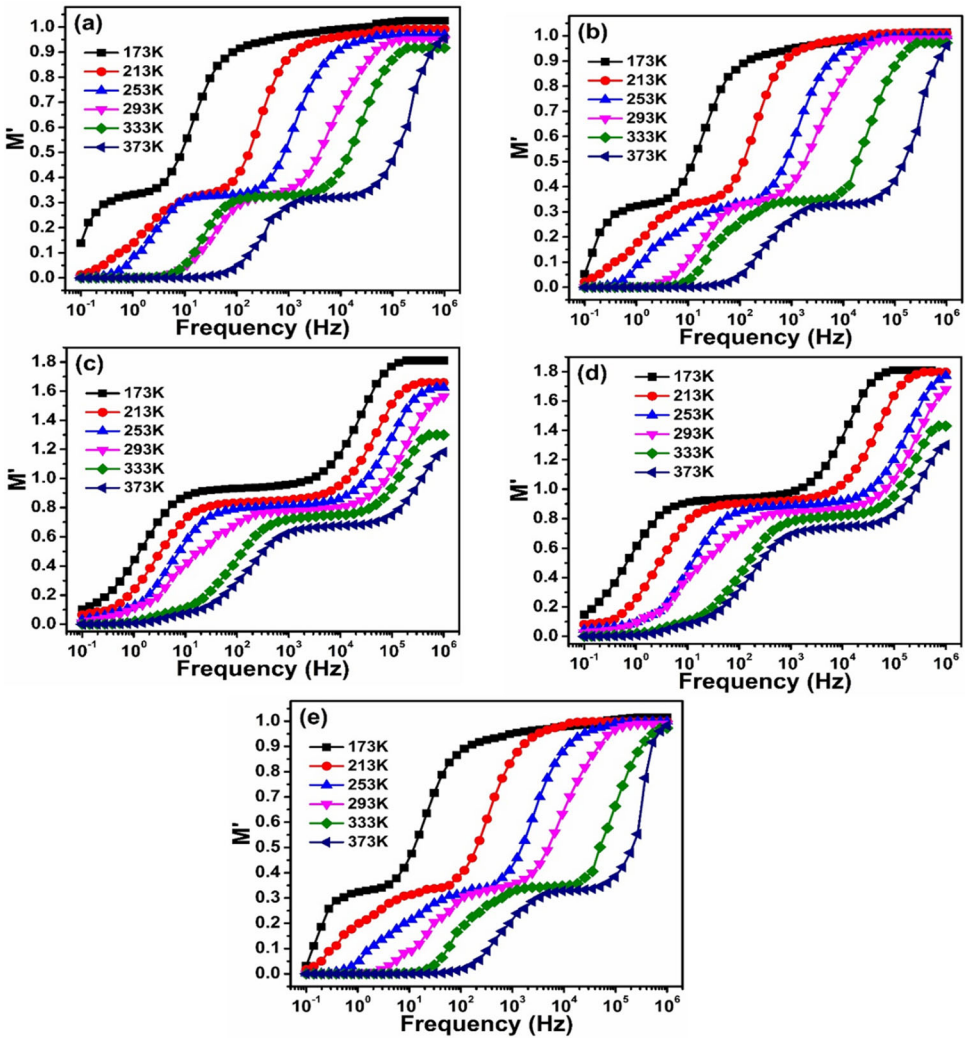

Fig. 9 Variation in the real function of the dielectric modulus as a function of logarithmic frequency at several temperatures for **a** pristine PANI, **b** 10 wt%, **c** 15 wt%, **d** 20 wt% and **e** 25 wt% $FeCl_3$ doped PANI

Here τ_m is relaxation time and β is the Debye-type relaxation deviation point. The updated KWW function is used to rationalize the electric modulus characteristic for the nanocomposite samples that is currently being manufactured. The imaginary portion of the electric modulus (M'') (plotted as Fig. 10a–e) with respect to this configuration can be written as [49]

$$M'' = \frac{M''_{\max}}{(1-\beta) + \frac{\beta}{1+\beta}\left[\beta\left(\frac{f_{\max}}{f}\right) + \left(\frac{f_{\max}}{f}\right)^{\beta}\right]} \quad (20)$$

where, $f_{\max}$ is the peak point frequency linked to the highest position of M'' i.e., $M''_{\max}$. The obtained practical values of M'' are theoretically fitted through the expression (20) and estimated the values of β and $f_{\max}$. The calculated values of β lies between 0.473 and 0.497.

The peak positions of M'' lifted towards the higher frequency side as temperature increases, indicating the temperature-dependent relaxation process. The charge carriers can move through the long range (dc conduction) before peak frequency whereas the charge carriers are restricted in the potential wells and assumed to be free in the frequency range after peak position of frequency. As a result, $f_{\max}$ marks change to long-range from short-range mobility.

4 Conclusions

Pristine and $FeCl_3$ doped PANI nanocomposite samples were prepared using the chemical oxidative polymerization method. The electrical dielectric characteristics of prepared pristine and composite samples were examined in the temperature range 173–373 K and frequency range 100 mHz to 1 MHz. Dielectric spectroscopic studies show that by doping $FeCl_3$ in the PANI matrix, the value of dielectric constant increases significantly from 497 to 875 at 100 mHz frequency. The charge transport properties of AC conductivity were studied through various models. Results show that the charge transport properties of AC conductivity follow Jonscher's universal power law. Arrhenius model indicates a strong relation between $\ln(\sigma_{dc})$ versus $1000/T$. From the temperature-dependent conductivity studies,

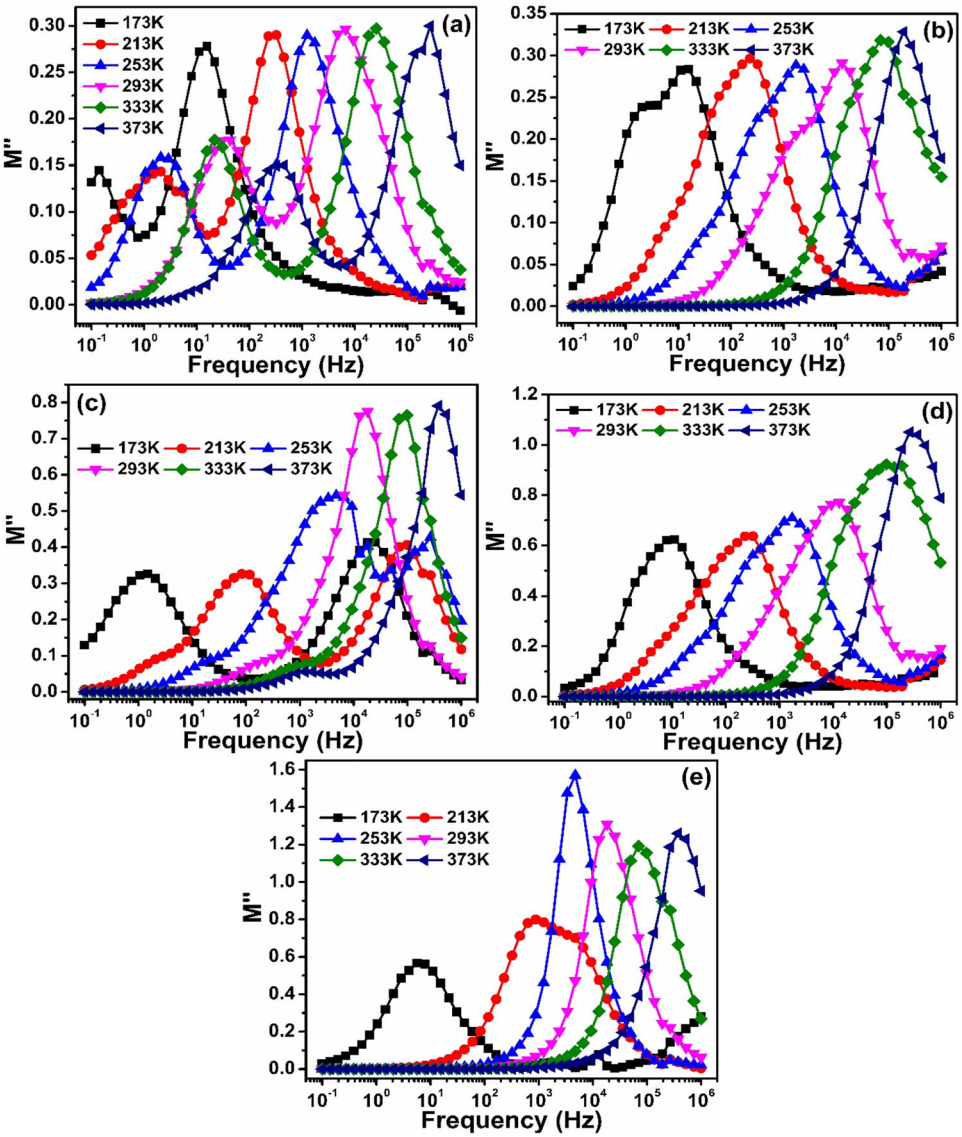

Fig. 10 Variation in the imaginary part of the dielectric modulus as a function of the logarithmic frequency at various temperatures for **a** pristine PANI, **b** 10 wt%, **c** 15 wt%, **d** 20 wt% and **e** 25 wt% $FeCl_3$ doped PANI

the values of σ_{dc} and ω_H were calculated for prepared samples which support the classical hopping mechanism of electrical conductivity in these samples. The lower values of H_f (lies between 1.93 and 2.51) and H_m (lies between 1.01 and 1.45) indicate the easy charge transport propagation in presently prepared samples. The values of β factor (Debye-type relaxation deviation point) lies in the range from 0.473 to 0.497. Dielectric spectroscopic studies show that by doping $FeCl_3$ in the PANI matrix, the value of the dielectric constant increases significantly from 497 to 875 at 100 mHz frequency. Due to such high value of dielectric constant for PANI-$FeCl_3$ composites, the composites could be a suitable candidate for application in energy storage, etc.

Acknowledgements The athors are grateful to GJUS&T, Hisar for providing the broadband dielectric/impedance spectrometer Novocontrol technologies for dielectric measurements.

Author contributions

Geeta Gulati: Conceptualization, investigation, methodology, writing—original draft. Meenakshi: Supervision, writing—review and editing. Asha: Supervision, validation, methodology, writing—review and editing. Rachna Dhankhar: Formal analysis. Sonia: Methodology. Rishi Pal: Writing—review and editing. Supreet: Formal analysis.

Data availability This manuscript has associated data in a data repository. [Authors comment: The data that support the findings of this study are available from the corresponding author upon reasonable request].

References

1. C. Yang, X. Wang, P. Du, P. Liu, Polyaniline/carbon nanotube multi-layered hollow microspheres with sandwich structure and their electrochemical performance. Synth. Met. **179**, 34 (2013). https://doi.org/10.1016/j.synthmet.2013.07.014
2. H. Xu, J. Zhang, Y. Chen, H. Lu, J. Zhuang, J. Li, Synthesis of polyaniline-modified MnO_2 composite nanorods and their photocatalytic application. Mater. Lett. **17**, 21 (2014). https://doi.org/10.1016/j.matlet.2013.11.089
3. B. Lai, P. Wang, H. Li, Z. Du, L. Wang, S. Bi, Calcined polyaniline-iron composite as a high efficient cathodic catalyst in microbial fuel cells. Bioresour. Technol. **131**, 321 (2013). https://doi.org/10.1016/j.biortech.2012.12.046
4. S.A. Umoren, M.M. Solomon, V.S. Saji, Conducting polymers, in *Polymeric Materials in Corrosion Inhibition*. (Elsevier, Amsterdam, 2022), pp.443–466. https://doi.org/10.1016/B978-0-12-823854-7.00002-3
5. D. Nguyen, H. Yoon, Recent advances in nanostructured conducting polymers: from synthesis to practical applications. Polymers **8**(4), 118 (2016). https://doi.org/10.3390/polym8040118
6. M.E. Abdelhamid, A.P. O'Mullane, G.A. Snook, Storing energy in plastics: a review on conducting polymers & their role in electrochemical energy storage. RSC Adv. **5**(15), 11611–11626 (2015). https://doi.org/10.1039/C4RA15947K
7. N. O. N. M. A. The Nobel Prize in Chemistry 2000, 2020. https://www.nobelprize.org/prizes/chemistry/2000/summary/.
8. T.H. Le, Y. Kim, H. Yoon, Electrical and electrochemical properties of conducting polymers. Polymers **9**(12), 150 (2017). https://doi.org/10.3390/polym9040150
9. W.J. Feast, J. Tsibouklis, K.L. Pouwer, L. Groenendaal, E.W. Meijer, Synthesis, processing and material properties of conjugated polymers. Polymer **37**, 5017 (1996). https://doi.org/10.1016/0032-3861(96)00439-9
10. A. Shimizu, K. Yamaka, M. Kohno, Rechargeable lithium batteries using polypyrrole–poly(styrenesulfonate) composite as the cathode-active material. Chem. Soc. Jpn. **61**, 4401 (1988). https://doi.org/10.1246/bcsj.61.4401
11. R. Pal, S.L. Goyal, I. Rawal, Asha, Lightweight graphene encapsulated with polyaniline for excellent electromagnetic shielding performance in X-band (8.2–12.4 GHz). Mater. Sci. Eng. B **270**, 115227 (2021). https://doi.org/10.1016/j.mseb.2021.115227
12. D. Braun, A.J. Heeger, Visible light emission from semiconducting polymer diodes. Appl. Phys. Lett. **58**, 1982 (1991). https://doi.org/10.1063/1.105039
13. S.B. Kulkarni, Y.H. Navale, S.T. Navale, F.J. Stadler, N.S. Ramgir, V.B. Patil, Hybrid polyaniline-WO3 flexible sensor: a room temperature competence towards NH_3 gas. Sens. Actuators B Chem. **288**, 279–288 (2019). https://doi.org/10.1016/j.snb.2019.02.094
14. S. Mezan et al., Synthesis and characterization of enhanced polyaniline nanoparticles by oxidizing polymerization. Solid State Technol. **63**, 256–266 (2020)
15. R. Mažeikienė, G. Niaura, A. Malinauskas, Raman spectroelectrochemical study of electrode processes at hybrid polyaniline-copper hexacyanoferrate modified electrode. J. Electroanal. Chem. **808**, 228–235 (2018). https://doi.org/10.1016/j.jelechem.2017.12.026
16. M. Jain, S. Annapoorni, Raman study of polyaniline nanofibers prepared by interfacial polymerization. Synth. Met. **160**, 1727–1732 (2010). https://doi.org/10.1016/j.synthmet.2010.06.008
17. M. Gautam, A.H. Jayatissa, Detection of organic vapors by graphene films functionalized with metallic Nanoparticles. J. Appl. Phys. **112**, 114326 (2012). https://doi.org/10.1063/1.4768724
18. A.H. Gemeay, I.A. Mansour, R.G. El-Sharkawy, A.B. Zaki, Preparation and characterization of polyaniline/manganese dioxide composites via oxidative polymerization: effect of acids. Euro Polym. J. **41**, 2575–2583 (2005). https://doi.org/10.1016/j.jcis.2006.12.077
19. I. Rawal, A. Kaur, Low-frequency and temperature-dependent dielectric spectroscopy investigations on polypyrrole nanoparticles. Philos. Mag. **95**, 1399–1413 (2015). https://doi.org/10.1080/14786435.2015.1031847
20. S. Banerjee, A. Kumar, Dielectric behavior and charge transport in polyaniline nanofiber reinforced PMMA composites. J. Phys. Chem. Solids **71**, 381–388 (2010). https://doi.org/10.1016/j.jpcs.2010.01.006
21. S.K.S. Parashar, S. Chaudhuri, S.N. Singh, M. Ghoranneviss, Electrical conduction in nanoceramic PGT synthesised by high energy ball milling. J. Theor. Appl. Phys. **7**, 267 (2013). https://doi.org/10.1186/2251-7235-7-26
22. I. Sakellis, A.N. Papathanassiou, J. Grammatikakis, Effect of composition on the dielectric relaxation of zeolite-conducting polyaniline blends. J. Appl. Phys. **105**, 064109 (2009). https://doi.org/10.1063/1.3097772
23. S. Dahiya, R. Punia, S. Murugavel, A.S. Maan, Conductivity and modulus formulation in lithium modified bismuth zinc borate glasses. Solid State Sci. **55**, 98–105 (2016). https://doi.org/10.1016/j.solidstatesciences.2016.02.013
24. R. Singh, A.K. Narula, R.P. Tandon, A. Mansingh, S. Chandra, Low frequency alternating current conduction and dielectric relaxation in polypyrrole, poly(*N*-methyl pyrrole), and their copolymers. J. Appl. Phys. **80**, 985 (1996). https://doi.org/10.1063/1.362911
25. W.Q. Ni, X.H. Zheng, J.C. Yu, Sintering effect on structure and dielectric properties of dielectrics $CaCu_3Ti_4O1_2$. J. Mater. Sci. **42**, 1037–11041 (2007)
26. R. Pal, S.L. Goyal, I. Rawal, V. Gupta, Dielectric characteristics of multiwall carbon nanotube-filled polyaniline. Mater. Chem. Phys. **297**, 127428 (2023)
27. K. Nath, K. Prasad, K.P. Chandra, A.R. Kulkarni, Impedance and a.c. conductivity studies of $Ba(Pr_{1/2}Nb_{1/2})O_3$ ceramic. Bull. Mater. Sci. **36**, 591–599 (2013). https://doi.org/10.1007/s12034-013-0503-y
28. R. Singh, A.K. Narula, R.P. Tandon, A. Mansingh, S. Chandra, Polaronic hopping conduction in poly(*N*-methyl pyrrole-pyrrole) copolymer. Philos. Mag. **75**, 419–430 (1997). https://doi.org/10.1080/13642819708202328
29. A. Mansingh, R.P. Tandon, J.K. Vaid, Dielectric relaxation in vanadium phosphate glasses. J. Phys. Chem.

Solids **36**, 1267–1271 (1975). https://doi.org/10.1016/0022-3697(75)90202-4
30. A. Dutta, A. Ghosh, Dynamics of lithium ions in calcium bismuthate glasses. J. Chem. Phys. **122**, 234510 (2005). https://doi.org/10.1063/1.1940636
31. R. Murugaraj, Ac conductivity and its scaling behavior in borate and bismuthate glasses. J. Mater. Sci. **42**, 10065–10073 (2007). https://doi.org/10.1007/s10853-007-2052-5
32. K. Funke, R.D. Banhatti, Conductivity spectroscopy covering 17 decades on the frequency scale. Solid State Ion. **176**, 1971–1978 (2005). https://doi.org/10.1016/j.ssi.2004.06.029
33. K. Funke, R.D. Banhatti, Ionic motion in materials with disordered structures. Solid State Ion. **177**, 1551–1557 (2006). https://doi.org/10.1016/j.ssi.2005.12.037
34. A.K. Jonscher, *Dielectric Relaxation in Solids* (Chelsea Dielectric Press, London, 1983). https://doi.org/10.1088/0022-3727/32/14/201
35. D.P. Almond, A.R. West, Anomalous conductivity pre factors in fast ion conductors. Nat. Lond. **306**, 456–457 (1983). https://doi.org/10.1038/306456a0
36. H. Jain, J.N. Mundy, Analysis of ac conductivity of glasses by a power law relationship. J. Non Cryst. Solids **91**, 315–323 (1987). https://doi.org/10.1016/S0022-3093(87)80342-3
37. R. Singh, A.K. Narula, R.P. Tandon, AC conductivity of poly(*N*-methylpyrrole). Synth. Met. **82**, 63–70 (1996). https://doi.org/10.1016/S0379-6779(97)80011-2
38. R. Singh, J. Kumar, R.K. Singh, A. Kaur, R.D.P. Sinha, N.P. Gupta, Low frequency ac conduction and dielectric relaxation behavior of solution grown and uniaxially stretched poly(vinylidene fluoride) films. Polymer **47**, 5919–5928 (2006). https://doi.org/10.1016/j.polymer.2006.06.023
39. A. Dey, S. De, A. De, S.K. De, Characterization and dielectric properties of polyaniline–TiO_2 nanocomposites. Nanotech **15**, 1277 (2004). https://doi.org/10.1088/09574484/15/9/028
40. G.E. Pike, AC Conductivity of scandium oxide and a new hopping model for Conductivity. Phys. Rev. B **6**, 1572 (1972). https://doi.org/10.1103/PhysRevB.6.1572
41. I.G. Austin, N.F. Mott, Polarons in crystalline and non-crystalline materials. Adv. Phys. **18**, 41–102 (1969). https://doi.org/10.1080/00018736900101267
42. N.K. Karan, B. Natesan, R.S. Katiyar, Structural and lithium ion transport studies in borophosphate glasses. Solid State Ion. **177**, 1429–1436 (2006). https://doi.org/10.1016/j.ssi.2006.07.032
43. N.F. Mott, *Conduction in Non-crystalline Materials* (Clarendon Press, Oxford, 1987). https://doi.org/10.4236/njgc.2011.12005
44. A. Ghosh, A. Pan, Scaling of the conductivity spectra in ionic glasses: dependence on the structure. Phys. Rev. Lett. **84**, 2188 (2000). https://doi.org/10.1103/PhysRevLett.84.2188
45. M. Dult, R.S. Kundu, J. Hooda, S. Murugavel, R. Punia, N. Kishore, Temperature and frequency dependent conductivity and electric modulus formulation of manganese modified bismuth silicate glasses. J. Non Cryst. Solids **423**, 1–8 (2015). https://doi.org/10.1016/j.jnoncrysol.2015.05.021
46. R. Vaish, K.B.R. Verma, Dielectric properties of Li_2O–$3B_2O_3Li_2O$–$3B_2O_3$ glasses. J. Appl. Phys. **106**, 064106 (2009). https://doi.org/10.1063/1.3225583
47. R. Kholrausch, Theorie des elektrischen Rückstandes in der Leidener Flasche. Pogg. Ann. Phys. **91**, 179–214 (1854). https://doi.org/10.1002/andp.18541670203
48. R. Bergman, General susceptibility functions for relaxations in disordered systems. J. Appl. Phys. **88**, 1356 (2000). https://doi.org/10.1063/1.373824
49. S.L. Asha, R. Goyal, R. Dhankhar, A. Sharma, Polyaniline chromium nitrate composites: influence of chromium nitrate on conductivity and thermal stability of polyaniline. Ind. J. Pure Appl. Phys. **12**, 982–988 (2022). https://doi.org/10.56042/ijpap.v60i12.66425